Extraction of seabed properties in mid-frequency range using waveguide invariant applied to broadband signals

Mohsen Badiey, Lin Wan, Christian David Escobar-Amado, et al.

Citation: Proc. Mtgs. Acoust. **45**, 070003 (2021); doi: 10.1121/2.0001532
View online: https://doi.org/10.1121/2.0001532
View Table of Contents: https://asa.scitation.org/toc/pma/45/1
Published by the Acoustical Society of America

Proceedings of Meetings on Acoustics

Volume 45 http://acousticalsociety.org/

181st Meeting of the Acoustical Society of America

Seattle, Washington

29 November - 3 December 2021

Underwater Acoustics: Paper 4aUW8

Extraction of seabed properties in mid-frequency range using waveguide invariant applied to broadband signals

Mohsen Badiey
Department of Electrical and Computer Engineering, University of Delaware, Newark, DE, 19716; badiey@udel.edu

Lin Wan, Christian David Escobar-Amado and Jhon Alejandro Castro-Correa
University of Delaware, Newark, DE, 19716; wan@udel.edu; escobarc@udel.edu; jcastro@udel.edu

One of the fundamental problems in shallow water environments is to assess the seabed properties. The waveguide invariant can be used in both passive and active sonar processing, source ranging, time reversal focusing, and in geoacoustic inversion processes. In Pekeris waveguide, the waveguide invariant value is approximately 1 and the slope of the interfering acoustic intensity fringes relates to the bottom sound speed. Using the slope of the striations as a variable, the spacing of the interference in range (or frequency) can be related to the penetration of energy into the bottom. The depth given by spacing of real arrivals has an effective depth of penetration which depends on the geoacoustic properties of the bottom sediments. Here, we study the frequency dependence of the waveguide invariant due to sediment layer structure and physical properties and provide a detailed data/model comparison for a shallow water range independent waveguide and extract the seabed properties for the frequency band 1.5 to 4.0 kHz using recent data obtained in shallow water environments.

Published by the Acoustical Society of America

 https://doi.org/10.1121/2.0001532

1. INTRODUCTION

The generalized acoustic shallow water waveguide, introduced by Pekeris in 1948,[1] has been a high-profile research topic in ocean acoustics. Due to advancements made in the recent decades, the solution to this problem now includes contributions of temporal and spatial variability of parameters and surface and seabed boundaries. This problem that relates to the remote sensing of waveguide properties has been a long-term challenge in the ocean acoustic community for which the extraction of geo-acoustic parameters is of particular interest. The principal objective is to assess the main parameters that have significant impact on the broadband acoustic signal propagation in shallow water environments.

In shallow water, the constructive and destructive interference is an inevitable consequence of multi-path acoustic propagation. If the ocean environment is sufficiently benign, the so-called waveguide invariant describes the resulting interference pattern.[2] The waveguide invariant, usually designated as β, has traditionally been regarded as a low-frequency phenomenon. The objectives of the present work is to examine the waveguide invariant for the mid-frequency range (1.5 to 4 kHz).

The waveguide invariant β describes striations presented in range-frequency spectrograms.[3] The invariant parameter depends on the frequency of the acoustic source, the distance between source and receiver, and to some degree on the Sound Speed Profiles (SSP) in the water column and the seafloor as well as the seafloor properties. The waveguide invariant parameter β is commonly used in both passive and active sonar processing, source ranging, time reversal focusing, and geo-acoustic inversion processes. In this paper, β is utilized to study the sound speed value at the water-mud interface and the gradient of the first mud layer.[4] Efforts are done to provide a detailed data-model comparison for a shallow water range-independent waveguide based on the Parabolic Wave Equation (PE).

The β parameter is commonly calculated considering the group and phase speed behavior of a pair of modes or taking into account the range- frequency-dependent striations shown in the spectrogram. However, much of the features needed to compute β must be hand-picked and represent a challenge when noise and artifacts are presented in the data. Image segmentation has been developed and widely used to extract meaningful features from data many decades ago.[5,6] Segmentation techniques such as adaptive thresholding can be used to overcome this issue by extracting features based on local intensity levels. In this paper, image segmentation is extended and applied to spectrograms for the extraction of representative patterns of β considering the local intensity levels exhibiting the spectrogram.

This paper is structured as follows. In section 2, the waveguide invariant parameter β is introduced. Section 3 shows the methodology used for geo-acoustic inversion. The measured and modeled data are shown along with the image segmentation process, and the inverse problem. Section 4 reports results obtained for the estimated sound speed at the top of the mud layer and gradient in the sediment, followed by conclusions in section 5.

2. WAVEGUIDE INVARIANT

The waveguide invariant β describes the acoustic interference patterns in a waveguide and is based on the dependence of phase slowness on group slowness, summarizing the robust interference phenomenon in the range-frequency plane. A first approach of the waveguide invariant parameter was published by Chuprov.[2] In Ref. [2], the waveguide invariant is explained in terms of normal modes and ray theory as well as how the waveguide invariant is related to range-frequency striations.[2,3] This theory was used to derive β for range-dependent and range-independent environments from measured broadband ship noise.[7] At long ranges the pressure spectrum of the recorded sound is a finite sum of normal modes. The spectrum is composed of two terms; the first term varies slowly with range and frequency, and the second term oscillates due to mode interference. The second term is responsible for the striation patterns and their slopes. According to D'Spain and Kuperman,[7] at a fixed frequency (f_0), the phase slowness difference is given by

$$\Delta S_p^{mn}(w_0) = \frac{1}{f_0 * (r_t - r_0)}, \tag{1}$$

where $(r_t - r_0)$ is the difference in range from the center of two adjacent striations. In the opposite direction of the spectrogram, at a fixed range (r_0), the group slowness difference can be computed as

$$\Delta S_g^{mn}(w_c) = \frac{1}{r_0 * (f_t - f_0)}, \tag{2}$$

where $(f_t - f_0)$ is the difference in frequency between two adjacent striations at a given instant in time.

Rouseff *et al.*,[8] modeled the waveguide invariant as a distribution. At various ranges and frequencies in the sound field, different groups of modes will be present and therefore the value of β will change as well. From normal mode theory the waveguide invariant can be calculated as the ratio of the phase slowness to group slowness, and both of these are associated with different modes. As a result β can be calculated as

$$\beta_{mn} = \frac{d\left(\frac{1}{v_m} - \frac{1}{v_n}\right)}{d\left(\frac{1}{u_m} - \frac{1}{u_n}\right)}, \tag{3}$$

where m and n are subscripts denoting separate normal modes of the waveguide, and $1/v$, $1/u$ are the modal phase and group slowness respectively. It is noted that both the modal phase and group slowness depend on sound speed, therefore, one can use β to estimate the sound speed at the water-sediment interface and the sound speed profile in the sediment.

Combining equations 1, 2 and 3, the waveguide invariant (β) can be expressed as

$$\beta = \frac{\Delta S_p}{\Delta S_g} = \frac{r_0}{f_0} * \frac{(f_t - f_0)}{(r_t - r_0)} \tag{4}$$

Harrison[9] used ray methods to demonstrate how changes in the SSP can affect the waveguide invariant parameter β. For certain upward and downward refracting profiles $\beta = -3$, while for isovelocity SSPs $\beta = 1$. An example of β calculation is shown in Fig. 1 where two adjacent striations at a range of 4.1 km and a center frequency of 2.29 kHz are selected from measured data in a nearly isovelocity SSP during the SBCEX 2017, yielding $\beta = 1.137$.

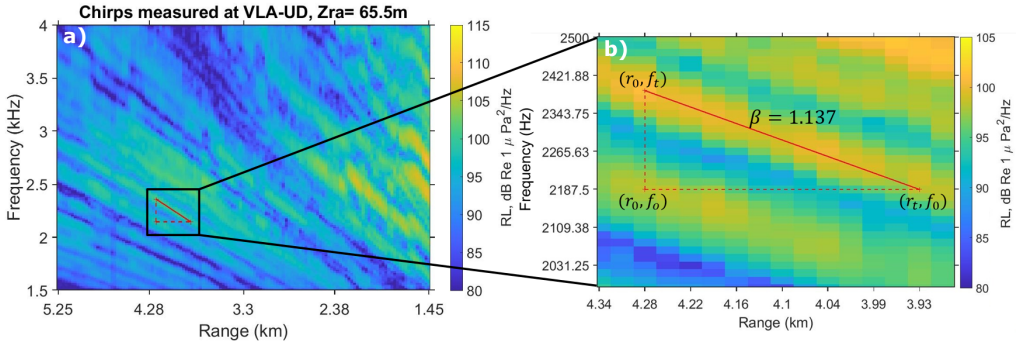

Figure 1: (Color online) (a) Computation of β on the chirps measured at VLA-UD on May 27. (b) Close-up of the β calculation in a range of 4.2807 - 3.9312 km and a frequency of 2.19 - 2.39 kHz.

3. METHODOLOGY

The methodology proposed for inferring the sound speed profile in the 10 m thick mud layer in shallow water environment is shown in Fig. 2. First, a set of random environmental parameters are selected to simulate a spectrogram using PE RAM.[11,12] Then, segmentation is applied to both, synthetic and measured signals, in order to extract the patterns that define the waveguide invariant parameter β. This process is repeated for N iterations, with $N = 100,000$. All the possible hypotheses $h \in \mathcal{H}$ corresponding to the PE synthetic data generated using PE are evaluated with respect to the measured data computing a cost function $E\left(c_p, g_{c_p}\right)$. The parameters of sound speed at the top of the mud layer c_p and its gradient in the sediment g_{c_p} yielding the lowest error between data and model outputs are considered the optimal values. Each part of this process is explained in detail throughout this paper.

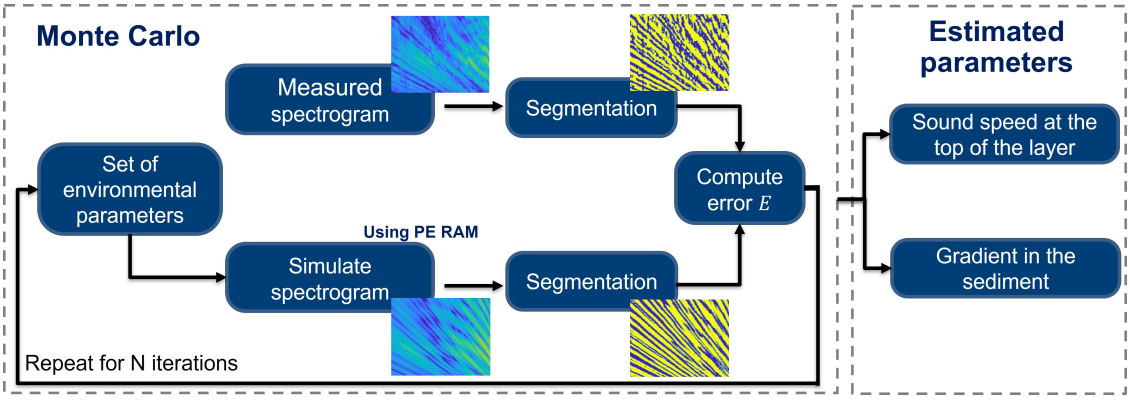

Figure 2: (Color online) Flowchart of the inversion algorithm used for obtaining the sound speed profile at the top of the mud layer and the gradient in the sediment.

A. MEASURED DATA

The data used in this paper were collected in the Seabed Characterization Experiment in 2017 (SBCEX 2017) in the New England Mud Patch Area.[10] The three vertical line arrays (VLA) shown in Fig. 3(a) were deployed by the Marine Physical Laboratory (MPL) of the Scripps Institution of Oceanography and by the University of Delaware (UD). For this work, only data collected at a single receiver in VLA-UD is employed. VLA1-MPL and VLA2-MPL are shown for reference. During a part of the SBCEX 2017, broadband linear frequency modulated (LFM) signals — also referred to as chirps — were transmitted in the 1.5 - 4 kHz frequency band by a towed source (ITC-2015) from Research Vessel (R/V) Endeavor. Transmissions consisted of 10 consecutive 1 s chirps followed by 10 s silence while ITC-2015 was tethered to the ship at the depth of $z_s = 45$ m below sea surface.

The piece of data used for this work was collected on March 27 from 16:31 to 17:14 UTC. The trajectory of the vessel while broadcasting the signals is shown in between points A and B by the blue line in Fig. 3(a). The water depth of the area is about 75 m with a slight change in bathymetry of less than 2 m in the ship track. The signal measured by VLA-UD at the receiver closest to the sea floor ($z_r = 65.5$ m) during this period is shown in Fig. 3(b). To account for the silence times, the chirps were extracted individually and then stacked to create a spectrogram representation in frequency versus range.

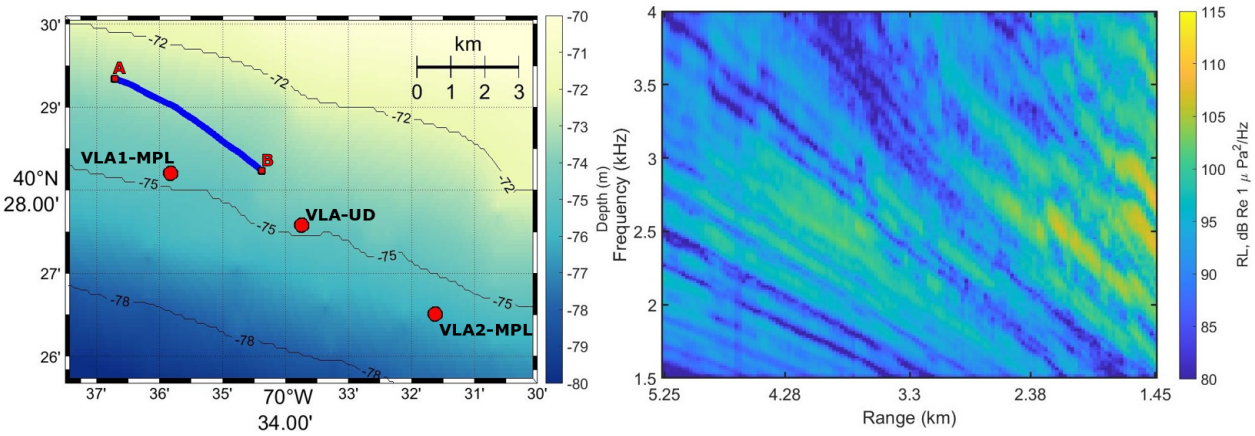

Figure 3: (Color online) (a) Map indicating the position of the ship while transmitting chirp signals (1.5-4.0 kHz). (b) Measured chirp signals emitted from ITC-2015 and received on VLA-UD from points A to B in (a). The source depth is at 45 m below the sea surface and the ship is moving at the speed of 1.54 m/s.

B. SYNTHETIC DATA

Data modelling is performed using the Range-dependent Acoustic Model (RAM), a parabolic equation (PE) solution of the acoustic wave equation developed by Collins.[11,12] The PE RAM model assumes a constant water density $p_w = 1$ g/cm^3, and only handles compressional waves in the ocean bottom. The input parameters needed to generate a broadband spectrogram using PE are the compressional sound speed profile in the water column c_w and sediment layers c_s (m/s), compressional attenuation in the water column α_w and sediment layers α_w (dB/λ), water depth h_w and layer thickness h_s (m), density in the sediment ρ_s (g/cm^3), frequency (Hz), maximum range $r_{\max}$ (m), range step size Δr (m), source depth z_s (m), and receiver depth (m). For PE RAM, compressional attenuation α_s in dB/m-kHz needs to be converted into dB/λ by multiplying α_s in dB/m-kHz by the speed of sound in its medium and dividing by 1000.

Given the nature of the almost-flat bathymetry profile exhibited during the SBCEX 2017, PE modeling of synthetic data was done considering a range-independent scenario across the path between points A and B depicted in Fig. 3(a) and using the fixed waveguide parameters shown in Table 1.

Table 1: Waveguide parameters used for modeling in PE RAM.

Waveguide parameter	**Value**
Water depth, h_w (m)	75
Water density, ρ_w (g/cm^3)	1
Receiver depth, z_r (m)	65.5
Source depth, z_s (m)	45
Maximum range, $r_{\max}$ (m)	5250
Range step size, Δr (m)	10

C. SEGMENTATION

Underwater acoustics inversions are commonly performed using techniques such as Matched Field Processing (MFP), Bayesian probabilistic methods, or gradient-based optimizations. In recent years, machine

learning and computer vision approaches have been successfully applied to underwater acoustics. By nature, spectrograms are represented as 2-dimensional matrices and can be seen as images for data analysis. As a result, image segmentation, a robust and high-developed approach, is used here for extraction of range- and frequency-dependent features from spectrograms. Image segmentation is a subset of computer vision and digital image processing, whose purpose is to group similar regions or segments of an image under different class labels. This technique encompasses both the classification and localization of patterns since regions of interest in data are localized and labeled according to pixel intensities.

Image segmentation can be accomplished using thresholding, clustering, or histogram-based methods.[5] In this paper, thresholding is selected to enhance and group different features found in spectrograms. Image segmentation via thresholding is performed by setting all pixels whose intensities are above a threshold to a foreground value and all the remaining pixels to a background value. The threshold used to segment images can be selected using histogram-shape, spatial, object-attribute, or adaptive methods. To adapt to the difference in intensities across the range and frequency axes in the spectrogram, and to guarantee a good feature extraction, adaptive thresholding is used in this paper.[6] In adaptive thresholding, local thresholds are calculated for small regions in the spectrogram, yielding different threshold values according to the intensity levels in the spectrogram.

Whereas the conventional thresholding operator uses a global threshold for all pixels, adaptive thresholding changes the threshold dynamically over the spectrogram. This more sophisticated version of thresholding can accommodate for range- and frequency-dependent features showed in spectrograms, e.g. those striations related to the wave invariant parameter β.

In this approach, adaptative thresholding is used to segment both the measured and modeled data. During the segmentation process, intensity levels in the spectrograms are treated the same way as pixel intensities in an image would be processed. Therefore, spectrograms are represented as $f(x, y)$, where x and y are the points in the range and frequency axes, respectively. Threshold values $h(x, y)$ across the spectrogram are computed by convolving the spectrogram $f(x, y)$ with a 2-dimensional Gaussian kernel $g(x, y)$ of size $n \times n$, where $n = 25$, as shown in Fig. 4(a)-(c). The Gaussian kernel $g(x, y)$ is built based on Eq. 5, such as

$$g(x, y) = \frac{1}{2\pi\sigma^2} e^{-\frac{x^2+y^2}{2\sigma^2}}, \tag{5}$$

where σ is the standard deviation. σ is calculated as $(n-1)/6$ for the kernel to cover more than the 99% of the Gaussian distribution. The resulting threshold values $h(x, y)$ (see Fig. 4(c)) are then used to segment the spectrogram $f(x, y)$ and generate Fig. 4(d). The foreground (1s in the segmented spectrogram) is selected such that the spectrogram level for the pixel x_i, y_i is greater or equal than the local threshold value $h(x_i, y_i)$, i.e., $f(x_i, y_i) \geq h(x_i, y_i)$. Conversely, the background (0s in the spectrogram) is chosen when the condition above does not hold, i.e., $f(x_i, y_i) < h(x_i, y_i)$.

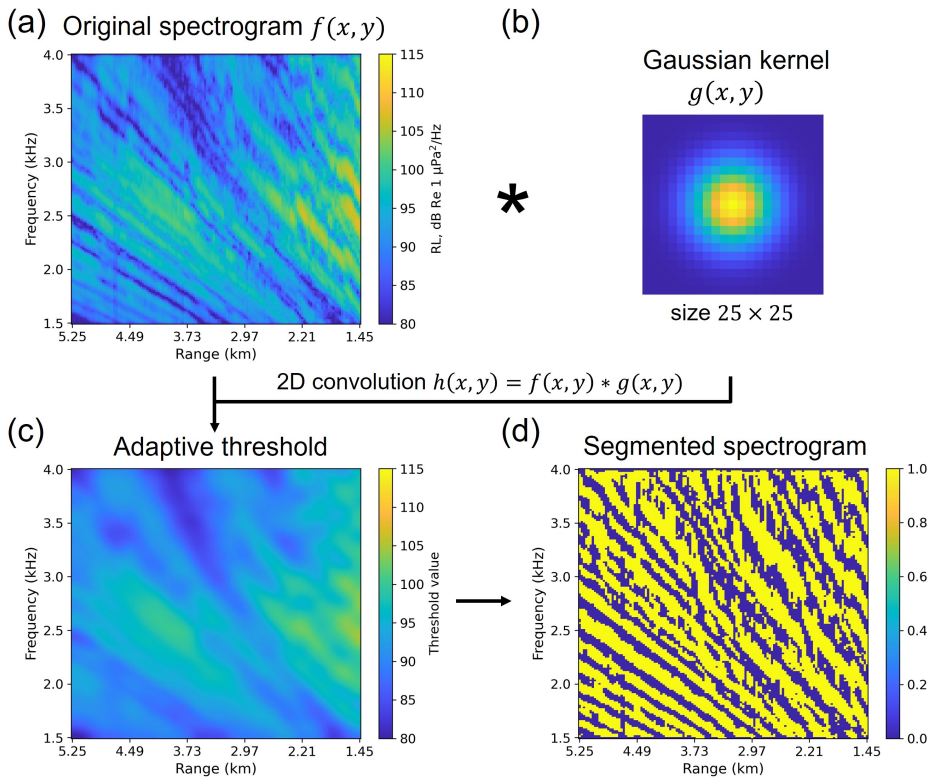

Figure 4: (Color online) Spectrogram segmentation with Gaussian kernel. The original spectrogram $f(x,y)$ ***in (a) is convolved with the gaussian filter*** $g(x,y)$ ***of size*** 25×25 ***shown in (b). The performed convolution yields a new matrix*** $h(x,y)$ ***with adaptive threshold values (c). Foreground in the segmented spectrogram in panel (d) is obtained by selecting the values greater or equal*** $(\geq)$ ***than the threshold at points*** x_i, y_i***.***

The segmentation procedure described in Fig. 4 is performed for measured and all the PE modeled data before the seabed parameters inversion via Monte Carlo simulation described in next sections.

D. INVERSE PROBLEM

Monte Carlo simulation is used to estimate the sound speed at the top of the mud layer c_p and the gradient in the sediment layer g_{c_p}. At each iteration, a random hypothesis is drawn from the possible sample space where the random and fixed geo-acoustic parameters are shown in table 2. For inversion, the sound speed in the mud sediment is assumed to be linear with a negative, null or positive gradient $g \in \mathbb{R}$. The bounds of this environment are graphically represented by the gray shadowed area in Fig. 5. The sound speed profile in the water column used to generate synthetic data was measured *in-situ* and exhibits a slightly upward refracting behavior.

Table 2: Random and fixed sediment parameters for the geo-acoustic inversion.

Parameter	**Mud Layer**	**Sand Layer**
Layer thickness, h_s (m)	10	100
Sound speed at the top of the layer, c_p (m/s)	1420 to 1485	1782
Sound speed gradient, g_{c_p} (s^{-1})	-5.0 to 25.0	0
Density the in sediment layer, ρ_s (g/cm^3)	1.66	2.1
Compressional attenuation, α_s (dB/m-kHz)	0.06	0.4

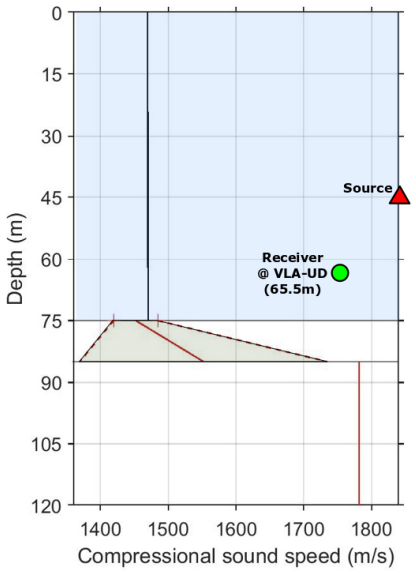

Figure 5: (Color online) Sound speed profile of the SBCEX 2017 shallow water waveguide. SSP in the water column is shown in the blue shadowed area. Sound speed bounds for the 10 m mud layer are represented by the gray shadowed area. The dashed lines indicate the minimum ($c_p = 1420\ m/s, g_{c_p} = -5\ s^{-1}$) and maximum ($c_p = 1485\ m/s, g_{c_p} = 25\ s^{-1}$) parameters for the speed in the mud layer.

Geo-acoustic parameter inversion for c_p and g_{c_p} is performed using the segmented version of measured and PE modeled data. The use segmented spectrograms for inversion allows extract relevant striation patterns related to the waveguide invariant parameter β, and discard any possible uncertainty in the source level of modeled data. The cost function used in this work is inspired in full waveform inversion techniques widely utilized to invert over seismic waveform raw samples.[14] The squared ℓ_2-error between the scaled segmented modeled spectrogram and the segmented observed data is defined as follows

$$E\left(c_p, g_{c_p}\right) = \frac{1}{2}\left\| \xi\left(\frac{\hat{\mathbf{y}}\left(c_p, g_{c_p}\right)\|\mathbf{y}\|_2}{\|\hat{\mathbf{y}}\left(c_p, g_{c_p}\right)\|_2} \right) - \xi\left(\mathbf{y}\right) \right\|_2^2, \tag{6}$$

where $\xi\left(\cdot\right)$ is the segmentation procedure described in Fig. 4, $\|\cdot\|_2$ is the ℓ_2-norm, $\hat{\mathbf{y}}\left(c_p, g_{c_p}\right)$ is the modeled data using PE RAM whose values depend on c_p and g_{c_p}, and $\mathbf{y}$ is the measured spectrogram at VLA-UD during the SBCEX 2017 experiment. Notice the term $\|\mathbf{y}\|_2/\|\hat{\mathbf{y}}\left(c_p, g_{c_p}\right)\|_2$ in the cost function is employed to adjust the amplitude of $\hat{\mathbf{y}}\left(c_p, g_{c_p}\right)$ with respect to $\mathbf{y}$ before segmentation.

Finally, the estimated sound speed at the top of the layer c_p^*, sound speed ratio, and sound speed gradient $g_{c_p}^*$ in the mud layer are calculated by selecting the hypothesis h^* that yields the lowest error $E(c_p^*, g_{c_p}^*)$

during the Monte Carlo simulation.

4. RESULTS

Details and results of the inversion of geo-acoustic parameters c_p and g_{c_p} via Monte Carlo simulation are discussed in this section along with the data-model comparison between the measured signal in the SBCEX 2017 and PE modeled spectrogram using the estimated sound speed and gradient in the mud layer.

A. MONTE CARLO SIMULATION

The sound speed at the top of the mud layer c_p, the sound speed ratio c_p/c_w, and the gradient of the sound speed in the sediment layer are estimated using a Monte Carlo simulation with $N = 100,000$ iterations. For each of the Monte Carlo iterations, the fixed values and bounds presented in Tables 1 and 2 are used to generate synthetic data with PE RAM. Random hypotheses h (modeled spectrograms) are uniformly drawn from the c_p and g_{c_p} bounds in Table 2, following an uniform distribution U, such that $h \sim U(\mathbf{u}, \mathbf{v})$ where $\mathbf{u}$ is a vector with the lower bounds and $\mathbf{v}$ are the upper bounds of c_p and g_{c_p} (see Table 2). The error $E\left(c_p, g_{c_p}\right)$, shown as surface plot in Fig. 6, is computed between each hypothesis $h = \hat{\mathbf{y}}\left(c_p, g_{c_p}\right)$ and the measured data $\mathbf{y}$.

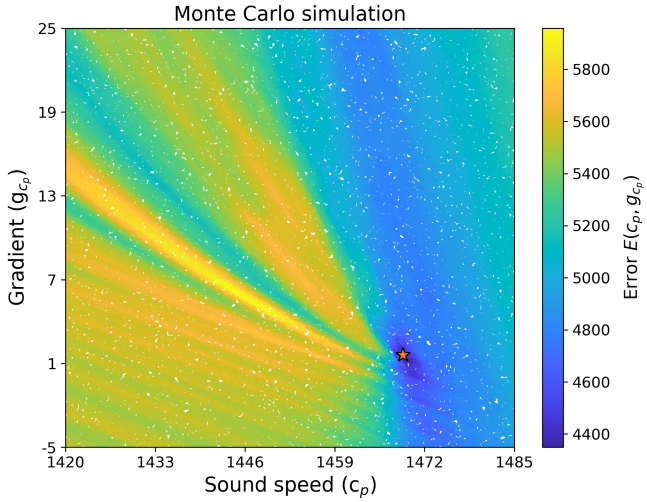

Figure 6: (Color online) Resulting error surface plot $E\left(c_p, g_{c_p}\right)$ for Monte Carlo simulation. x axis is the sound speed profile at the top of the sediment layer (c_p), whereas the y axis shows the sound speed gradient in the sediment (g_{c_p}). The lowest error $E\left(c_p^*, g_{c_p}^*\right)$ is demarcated as an orange star.

It is clear there exists a correlation between the sound speed at the top of the mud layer c_p and the gradient in the sediment g_{c_p} since the error surface plot shown in Fig. 6 presents a nearly-linear dependence between the both inverted parameters. The majority of local minimums in the cost function $E\left(c_p, g_{c_p}\right)$ are presented for values c_p in the range from 1470 to 1475 m/s, indicating that the sound speed ratio between the mud layer and the water column is close to 1. The values of c_p^* and $g_{c_p}^*$ that yield the global minimum in the cost function $E(c_p^*, g_{c_p}^*)$, among the hypotheses h generated with the 100,000 Monte Carlo iterations, are marked with an orange star in Fig. 6. The estimated sound speed at the top of the mud layer is $c_p^* \approx 1,468.9$ m/s, yielding a sound speed ratio (c_p/c_w) between the sediment and the water column of 0.9985, while the estimated sound speed gradient in the sediment is $g_{c_p}^* \approx 1.61$ s$^-1$.

The parameters reported in this paper are preliminary and require further research. However, these values agree with previous work in which the sound speed ratio inverted in the experimental area was about ~ 1 and the sound speed gradient in the mud layer shown to be in the range from 0 to 2 s^{-1}.[15–17]

B. DATA-MODEL COMPARISON

The estimated sound speed at the top of the mud layer c_p^* and gradient in the sediment $g_{c_p}^*$ were used to generate the PE modeled spectrogram that best resemble the measured data at VLA-UD channel 8 ($z_r = 65.5$ m) during the SBCEX 2017. A data-model comparison between the measured and modeled data is presented in Fig. 7 using all the parameters shown in Tables 1 and 2.

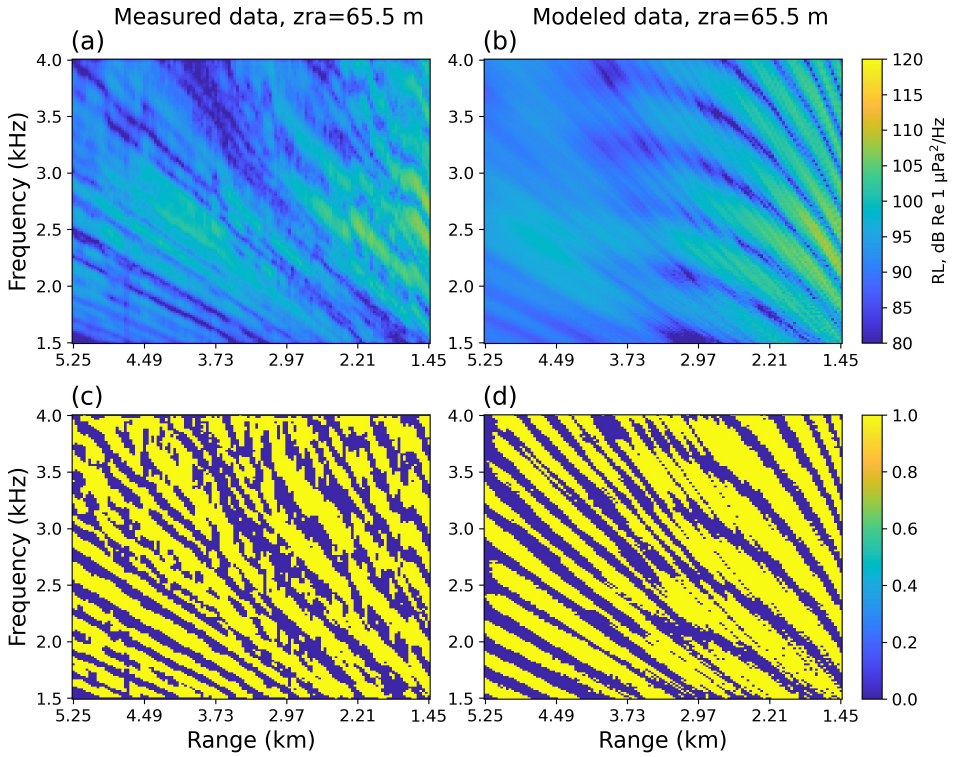

Figure 7: (Color online) Data model comparison of inversion using the optimal value from Monte Carlo simulation. (a) The received level measured by VLA-UD at $z_{ra} = 65.5$ m. (b) Modeled received level generated by PE RAM using the optimal values $\hat{c}_p$ and $\hat{g}_{cp}$. (c) Segmented spectrogram of the measured data shown in panel (a). (d) Segmented spectrogram of the modeled spectrogram in (b).

Panels (a) and (b) in Fig, 7 compare the measured data versus the model generated with PE RAM, respectively. The segmented spectrograms in Fig. 7(c)-(d) allow a better comparison between the range- and frequency-dependent striation patterns presented in Fig. 7(a) and (b). Even though the patterns corresponding to the waveguide invariant β in the modeled spectrogram (see Fig. 7(a)) seems to vanish after 3 km in range, it is clear that those are still present in Fig. 7(d) and describe similar trends than the segmented measured data in Fig. 7(c). As a result, image segmentation for feature extraction demonstrates to be useful for inversion and the picking of β-like striation patterns. The methodology presented in this paper is exploratory, and further analyses need to be done to fine-tune the results.

5. CONCLUSIONS

This study was motivated by chirp data transmitted in the frequency band of 1.5 to 4 kHz and measured at VLA-UD in the SBCEX 2017 deployed by the University of Delaware. Image segmentation was used to extract relevant features in the data by treating the spectrograms as images to detect the presence or absence of range- and frequency-dependent striations patterns related to the waveguide invariant parameter β. For the inverse problem process, the cost function — squared ℓ_2-error — was computed with respect to the segmented measured and synthetic spectrograms rather than with respect to the received levels. This way, uncertainty in the source level does not affect the computations since only the position of the striations are considered, which ultimately is determined by the value of β.

When using this technique, the estimated geo-acoustic parameters that yielded the global minimum in the cost function were $c_p^* \approx 1,468.6$ m/s in the case of sound speed at the top of the mud layer, corresponding to a sound speed ratio of 0.9985, and $g_{c_p}^* \approx 1.61$ s^{-1} for the gradient in the sediment. In some previous work, the sound speed ratio has been hypothesized to be close 1 whereas the gradient in the sediment (g_{c_p}) has been reported in a range from 0 to 2 s^{-1}.[16,17] The estimated values for c_p, sound speed ratio and g_{c_p} reported in this paper correspond to preliminary results for this specific piece of data measured at a single receiver, and further analyses are yet to be done.

ACKNOWLEDGMENTS

This research was supported by ONR Grants N00014-21-1-2760 and N00014-21-1-2424. Authors acknowledge the R/V Endeavor's crew and all the participants of the SBCEX 2017 experiment.

REFERENCES

[1] C., L. Pekeris, "Theory of propagation of explosive sound in shallow water", *Geol. Soc. Am.* **27**, pp. 1-117 (1948).

[2] S. Chuprov, "Interference structure of the sound field in a stratified ocean", *in Ocean Acoustics.* Current Status, edited by L. M. Brekhovskikh, Moscow, pp. 71-91 (1982).

[3] K. L. Cockrell, "Understanding and utilizing waveguide invariant range-frequency striations in ocean acoustic waveguides", *Massachusetts Inst. Tech. Cambridge* (2011).

[4] M. Badiey, L. Wan, C. D. Escobar-Amado, J. A. Castro-Correa. "Extraction of seabed properties in mid-frequency range using waveguide invariant applied to broadband signals," *J. Acoust. Soc. Am.* **150(4)**, pp. A281-A281 (2021).

[5] R. M. Haralick, and L. G. Shapiro, "Image segmentation techniques", *Computer vision, graphics, and image processing* **29(1)**, pp. 100-132 (1985).

[6] S. S. Al-Amri, N. V. Kalyankar, and S.D. Khamitkar , "Image segmentation by using threshold techniques", J. of Computing. **5(2)**, pp. 83-86 (2010).

[7] G. L. D'Spain, W. A. Kuperman, "Application of waveguide invariants to analysis of spectrograms from shallow water environments that vary in range and azimuth", *J. Acoust. Soc. Am.* **106(5)**, pp. 2454-2468 (1999).

[8] D. Rouseff, and R. Spindel, "Modeling the waveguide invariant as a distribution", *AIP conference Proceedings* **621**, pp. 137-150 (2002).

[9] C. H. Harrison, "The Waveguide Invariant: Spatial Interference Patterns in Underwater Acoustics", *Acoustics Today* **p(3)**, pp. 39-43 (2013).

[10] S. W. Preston, D. P. Knobles, and T. B. Neilsen, "Guest Editorial An Overview of the Seabed Characterization Experiment", *IEEE J. Oceanic Eng* **45(1)**, pp. 1-13 (2020).

[11] M. D. Collins, "A split-step Padé solution for the parabolic equation method", *J. Acoust. Soc. Am.* **93**, pp. 1736-1742 (1993).

[12] M. D. Collins, "Generalization of the split-step Padé solution", *J. Acoust. Soc. Am.* **96**, pp. 382-385 (1994).

[13] H. Ngodock, M. Carrier, J. Fabre, R. Zingarelli, and I. Souopgui, "A variational data assimilation system for the range dependent acoustic model using the representer method: Theoretical derivations", *J. Acoust. Soc. Am.* **142**, pp. 186-194 (2017).

[14] J. O. Serrano, A. B. Ramirez, S. A. Abreo, and B. M. Sadler,"Alternative cost function for full waveform inversion of GPR data," *Proc. SPIE.* **11418**, 1141806 (2020).

[15] L. Wan, M. Badiey, D. P. Knobles, and P. S. Wilson, "The Airy phase of explosive sounds in shallow water", *J. Acoust. Soc. Am.* **143(3)**, pp. EL199–EL205 (2018).

[16] L. Wan, M. Badiey, D. P. Knobles, P. S. Wilson, and J. Goff, "Estimates of low-frequency sound speed and attenuation in a surface mud layer using low-order modes," *IEEE J. Ocean Eng.* **45**, pp. 201–211 (2020).

[17] C. W. Holland, "Sound speed gradients in mud," *J. Acoust. Soc. Am. Express Letters* **1(6)**, 066001 (2021).